An e-BAS Optimized *d-q* Controller for Grid Voltage Stability of Single Stage Solar PVS with PQ Disputes

P. Meganathan*‡, C. Sasi**, P. Pugazhendiran***, P. Nammalvar****

*Department of Electrical Engineering, Research Scholar, Annamalai University, Chidambaram, Tamilnadu, India – 608002

**Department of Electrical, FEAT, Annamalai University, Chidambaram, Tamilnadu, India – 608002

***Department of Electrical and Electronics Engineering, IFET College of Engineering, Villupuram, Tamilnadu, India – 605108

****Department of Electrical and Electronics Engineering, Krishnasamy College of Engineering and Technology, Cuddalore, Tamilnadu, India – 607109

(megaisagem@gmail.com, saasi_ceee@yahoo.co.in, pugazhendiran@gmail.com, alvar1976@gmail.com)

‡Corresponding Author: Mr. P. Meganathan, Assistant Professor/EEE, Sri Venkateshwaraa College of Engineering and Technology, Ariyur, Puducherry, India – 605102, Tel: +91 8870984192, megaisagem@gmail.com

Received: 06.04.2023 Accepted:24.06.2023

Abstract- An escalating solar Photovoltaic System (PVS) with grid integration is the most common solution for auxiliary power demands. Despite its benefits, operating solar PVS under fast varying environmental conditions with nonlinear loads is the most challenging job. Almost, the grid integration with solar PVS provides active power at Maximum Operating Point (MOP) and also reactive power compensation without affecting the grid voltage stability. Consequently, a holistic single-stage solar PVS is considered for harvesting solar power at variability conditions as a proposed system. This controls the voltage stability of the grid by the reactive power compensation based on the *P-Q* capability curve. Also, it eliminates the overshoots of voltage and current with reduced distortion at non-linear loads. A fruitful enhanced Beetle Antenna Search (e-BAS) tuned *d-q* controller is proposed and implemented for deterministic grid integration of solar PVS to enhance the reactive power control with minimum distortions. The ability of the proposed controller has been assessed through MATLAB/Simulink environments. The simulation illustrations conclude that e-BAS tuned *d-q* controller reveals the betterment of grid integration solar PVS.

Keywords Reactive power; *d-q* controller; voltage source inverter; solar photovoltaic; grid voltage stability; BAS algorithms.

1. Introduction

In recent years, the growth of the population has increased, and also electricity demand rises with the development of power electronics applications. These demands for electricity are distributed by non-conventional sources namely hydro energy, wind energy, solar energy, bio-energy, and geothermal energy [1], [2]. The International Renewable Energy Agency (IRENA) March 2022 released the statistics key data for global renewable generation capacity in GW is reported in Fig. 1. Among the RESs solar PVS has elegant benefits like no fuel, noise-free, pollution-free, etc. which raises the growth of solar PVS in the field of power generation. The large solar PVS are connected to the grid in order to supply the electricity demands. The grid integration solar PVS undergoes active power and reactive power for secondary services such as improvement in grid power quality, grid voltage stability, compensation of reactive power, etc.

In [3] classify the reactive power control techniques for the voltage regulation in high Photovoltaic (PV) power penetrations to resolve the shortcoming of voltage rise disputes. Whereas [4], [5] highlights the reactive power booster resource the grid voltage at voltage sag which constrains the grid-connected inverters. In [6] focused on a

grid-tied inverter for reactive power compensation to affirm the grid voltage with the control techniques of the inverter for the balanced operation of the grid integration. But [7], [8] employed the control method to control the inverter using a proportional-integral-resonant compensator for the constant active power in the grid.

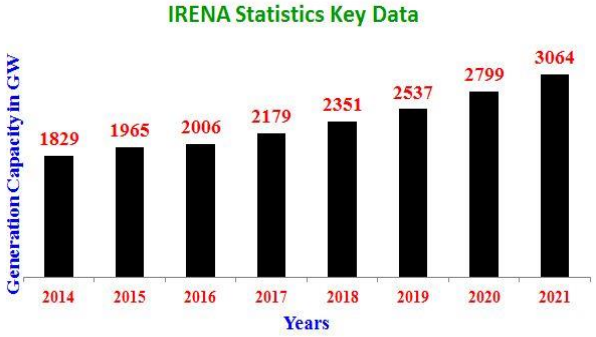

Fig. 1. IRENA Statistics key data for global generation capacity in GW.

In [9] compares the performance of inverter with *d-q* controller for different meta-heuristic algorithms to achieve the efficiency, stability, and dynamic response of grid-connected solar PVS. Whereas, [10] presents the grid-tied inverter with the *d-q* controller by intelligent fuzzy base control algorithms to achieve real and reactive power support to the grid integration. In [11] proposed the slide mode controller for a grid-connected inverter with *d-q* controller techniques with reduced harmonics and overall current distortions with minimum overshoots. Similarly [12] compares the grid inverter with the backstepping techniques along with the slide mode controller and vector control methods for injecting active and reactive power to the grid integration.

In [13], [14] implemented the controller uses the modulation index of the inverter and the load angle of grid integration. It achieves fast-tracking responses with real and reactive power compensations through the Voltage Sources Inverter (VSI). However, [15] influence the generation of reactive power through the solar PVS inverter with reduced system losses. It can be achieved by increasing the overall system loading with the unity power of the inverter. In [16] develops the reliability under grid fault conditions for a double-stage grid integration PVS. It shoots up solar PVS power into the grid by disabling the driving point control to reduce the outcomes of the inverter. Later it releases high performances during the transient and the occurrences of grid faults. Where [17] present the topology for NPC inverter with state space analysis. It motivates the design and modeling of the three-phase NPC inverter controller resulting to maintain the DC voltage and proper tracking responses.

In [18] proposes the compensation of reactive power by preventing unintentional fluctuations in the reactive power flow. It measured the grid impedance to mitigate Power Factor (PF) control and the reactive power fluctuation for better transmission flow. Although, [19] intended system gives an efficient solution for reactive power compensation using a new active distribution network. It also reduces operating losses with improved voltage levels at balanced system accuracy and better efficiency. In [20] proves the active and reactive power performance at double-stage grid integrations in solar PVS. The simple algorithm of slide mode control with direct power control provides good results in both steady and transient states. But, [21] present a non-linear control method called feedback linearization to reduce the nonlinearity and disturbance existing in the solar PVS. The linear matrix constraints with D-stability criteria and state-feedback benefits for the improvement of system response are applied to the controller to reduce the perturbation and interferences.

In [22], [23] investigates the reliability of active and the reactive power of solar PVS. To avoid voltage destruction from the system failure the reactive power shortage is compared to the real power shortage for the different load scheduling. Appropriately, the reactive power reduced the risk impact of reliability in solar PVS. However, [24], [25] achieves reactive power regulation through the grid-tied inverter of solar PVS. The 30 MW solar PVS is compared to the theoretical analysis of solar PVS without compensating devices for reactive power capacity. Also, the results are achieved in controlling voltage and PF with its system efficiency. In [26] presented the techniques to restore unknown reactive power value from the grid-connected solar PVS. This technique uses non-linear least squares and manual tuning for filters. It results are compared with the conventional active power that is separated from other techniques. But [27] discusses a novel modulation technique to improve the DC regulation of solar PVS by compensating reactive power. It results are achieved by less compensation of reactive power with reduced switching events.

Based on the prior studies the collected hand-outs of solar PVS are that the variability of solar power harvesting failed to include in the grid stability, also the power generation does not follow the holistic approaches in grid-tied solar PVS. The probabilistic of the grid integration in solar PVS is assessing the voltage stability for limited low-power generation [28], [29]. However, studies include the semblance of deterministic in reactive power compensation without considering a capability curve during the interchange of grid power. Moreover, it failed to deliver the impact of variable loads, grid current, and THDs performance in the grid-tied solar PVS. The recent studies create negative effects due to the presence of nonlinear load and the impact of overshoot in voltage and current during the behaviour of dynamic analysis.

In the essence of the above studies, this research work arises an approach for a holistic evaluation of grid integration solar PVS. The variability due to the fast varying environmental conditions has been considered in the proposed system for solar power harvesting and the voltage stability is controlled by the real and reactive power compensation at the Maximum Operating Point (MOP). The reactive power compensation of the proposed system is limited by the Q_{max} and Q_{min} based on the *P-Q* capability curve. Also, the proposed solar PVS have been analysis the grid behaviour in terms of grid current and THDs at variable nonlinear loads. The impact of voltage and current overshoot has been eliminated by the proposed system. In this regard,

an enhanced Beetle Antenna Search (e-BAS) tuned *d-q* controller is considered the proposed system, and the Analysis of Variance (ANOVA) tuned *d-q* controller is considered a conventional system. The conventional system is chosen based on the prior study of various techniques in solar PVS and ended ANOVA from statistical method which is not in meta-heuristic algorithms.

Intention for the choice of proposed system is, in [30] presented the BAS algorithms for tuning the PID controller to upgrade the competence of the proposed system. Whereas [31] explains that the BAS method achieved the exploration and exploitation also, the outcomes are better in respect of accuracy, stability, and robustness. Moreover, [32] implement the BAS procedure for enhancement of maximal power tracking under non-uniform shading conditions. However, BAS technique [33] succeeds overloading in the grid at peak power generation with less complexity of solar PVS.

The organizations of this research work progress; Section 2 discusses the contest of solar PVS and its beliefs. Section 3 disputes the implementation of the proposed controller and the simulation results and its explanation is portrayed in Section 4. As a final point, a conclusion reveals the perfection of the research progress.

2. Formularized Approach of Solar PVS

The grid integration of solar PVS consider as a proposed system is represented in Fig. 2.

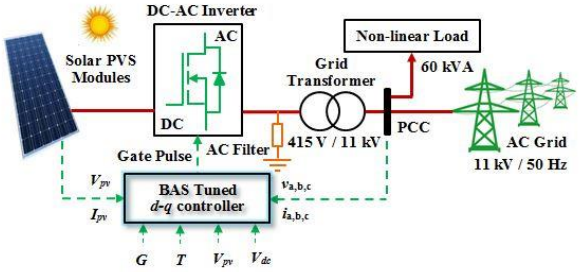

Fig. 2. A simple layout diagram of grid integration solar PVS.

This solar PVS is a single-stage system consisting of solar PVS cells in modules on the PV side and a VSI with a proposed *d-q* controller on the grid side. The illustration of solar PVS activates the intended e-BAS tuned *d-q* controller. On the grid connected VSI with e-BAS tuned controller gains the value of controller to regulate the MOP *i.e* Maximum Power Point Tracking (MPPT) and to regulate maximum active and reactive power into the grid. Table 1 specifies the parameter identification of the solar PV panel considered in the proposed system.

2.1. ANOVA Technique

Professor R.A. Fisher developed the Analysis of Variance (ANOVA) theory as a statistical method [34]. The ANOVA methods are used in more than a few areas in sociology, psychology, finances, etc. The conventional ANOVA technique is an optimization way out by "population" in the preliminary group of the data which determines by the value of the *F-table*. The optimum ANOVA techniques run through assured practices of numerical theory tests by relating the premeditated value of the *F-ratio* value to the *F-limit* value for the decision of an alternative hypothesis (H_A) or null hypothesis (H_0). The summarization of one-way ANOVA steps [35] is specified in Fig. 3.

Table 1. Identification of solar PVS cell

Description	Ratings
Number of cells in series	ncells = 72
Optimal voltage, V	V_{max} = 37.1 V
Optimal current, A	I_{max} = 8.62 A
Optimal power, W	P_{max} = 320 W
Short circuit current, A	I_{sc} = 9.08 A
Open circuit voltage, C	V_{oc} = 45 V

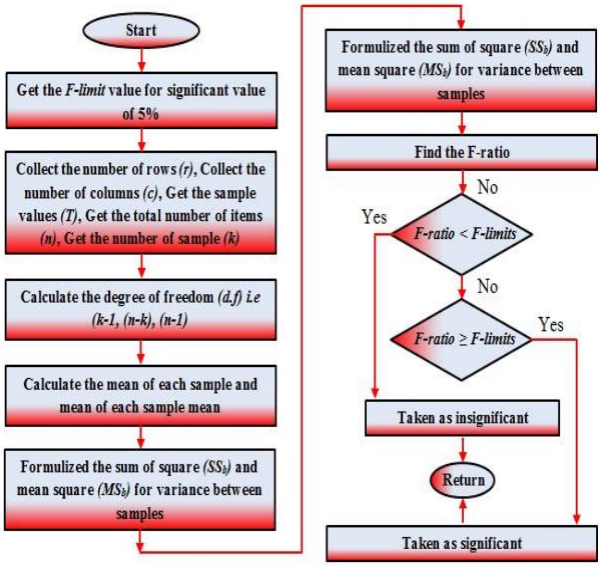

Fig. 3. Summarization of ANOVA technique in flowchart.

2.2. BAS Technique

The coleopteran family includes a beetle that has two lengthy antennae for forage and also to odour the prey. When beetles sense a higher odour of prey through antennae on the right side it would travel toward the same direction *i.e* right side. Similarly, when beetles sense the other side on the left side they would travel toward the opposite direction *i.e* left side. Based on this forage, the beetle reaches the least length from the position to succeed in the optimum solution. The searching action is exhibited as a Meta-heuristic technique as

Beetle Antenna Search (BAS) technique and its habitual searching behaviour is shown in Fig. 4.

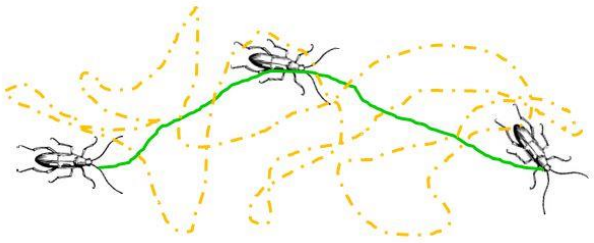

Fig. 4. Beetle searching behaviour.

The various step involved in BAS technique is specified by stages as:

Stage 1: *f[p(t)]* is the objective function of the BAS technique where *p(t)* represents the precise beetle position at time '*t*'. The optimum value *f[p(t)]* is attained by recurs of high odor foraging.

Stage 2: $p_m(t)$ is the random position of beetles in the M^{th} position where $m = 1, 2, \ldots..M$. Initially iteration set as $j = 0$ to j_{maxi} is the maximum of iteration.

Stage 3: The searching of beetle antennae in a direction at initial exploration is normalized by

$$\vec{e} = \frac{rand(\dim s,1)}{\|rand(\dim s,1)\|} \tag{1}$$

where, $\vec{e}$ – is the vector unit direction, $rand$ – represents a random function, $\dim s$ – denotes a structural space in the searching path, and $\|.\|$ – specifies the normalization.

Stage 4: The higher odor sensed by beetle antennae from neither the right side nor the left side is normalized by

$$p(t)_r^j = p(t)^j + d^j.\vec{e} \tag{2}$$

$$p(t)_l^j = p(t)^j - d^j.\vec{e} \tag{3}$$

where, $p(t)_r^j$ and $p(t)_l^j$ – indicates the precise position of beetles right and left respectively at j^{th} iteration, $p(t)^j$ – indicates the precise position of beetle at j^{th} iteration, d^j – indicates the antennae sensing length at j^{th} iteration, and j – indicates the count of iteration $j = 0$ at initially.

Stage 5: When foraging progresses in higher odor beetle moves to the next precise position neither the right side nor left side is given by

$$p(t)^{j+1} = p(t)^j + z.\delta^j.\vec{e}.sign\left(p(t)_r^j - p(t)_l^j\right) \tag{4}$$

where, z – indicates the direction of the beetle's movement, δ^j – indicates the change in step size of beetles movement in j^{th} iteration and $sign(.)$ – indicates the sign is specified by

$$sign(d\Delta) = sign\left(p(t)_r^j - p(t)_l^j\right) = \left.\begin{array}{l|l} (d\Delta) > 0 & 1 \\ (d\Delta) = 0 & 0 \\ (d\Delta) < 0 & -1 \end{array}\right\} \tag{5}$$

Stage 6: The foraging detecting length through antennae d^j and the changing step size while searching δ^j can be remodeled as

$$d^{j+1} = \psi_1.d^j + 0.01 \tag{6}$$

$$\delta^{j+1} = \psi_2.\delta^j \tag{7}$$

where, ψ_1 and ψ_2 – lies between 0 and 1 known as reduction factor (commonly a constant)

2.3. BAS Technique

Fig.2 illustrates the layout diagram of solar PVS with a *d-q* controller. At PCC, the measured per-phase voltage is denoted by $V_{a,b,c}$ which is revealed by the output of VSI voltage as $V_{a0,b0,c0}$.

The balanced voltage equation is given by equation (8)

$$\begin{bmatrix} V_a \\ V_b \\ V_c \end{bmatrix} = R_1 \begin{bmatrix} i_a \\ i_b \\ i_c \end{bmatrix} + L_1 \begin{bmatrix} \Delta i_a \\ \Delta i_b \\ \Delta i_c \end{bmatrix} + \begin{bmatrix} V_{a0} \\ V_{b0} \\ V_{c0} \end{bmatrix} \tag{8}$$

By equation (8), the balanced equation of voltage and current in the *d-q* transformation is given by (9) and (10)

$$\begin{bmatrix} V_d \\ V_q \end{bmatrix} = R_1 \begin{bmatrix} i_d \\ i_q \end{bmatrix} + L_1 \begin{bmatrix} \Delta i_d \\ \Delta i_q \end{bmatrix} + \omega L_1 \begin{bmatrix} -i_q \\ i_d \end{bmatrix} + \begin{bmatrix} V_{d1} \\ V_{q1} \end{bmatrix} \tag{9}$$

$$\begin{bmatrix} i_d \\ i_q \end{bmatrix} = \begin{bmatrix} i_{d1} \\ i_{q1} \end{bmatrix} + C_1 \begin{bmatrix} \Delta V_{d1} \\ \Delta V_{q1} \end{bmatrix} + \omega C_1 \begin{bmatrix} -V_{q1} \\ V_{d1} \end{bmatrix} \tag{10}$$

where, V_{d1} and V_{q1} – are the voltage in the *d-q* transformation at PCC, V_d and V_q – are the output voltage of the inverter in the *d-q* transformation, R_1 and L_1 – are the resistance and inductance of the AC filter and ω – is the angular frequency of voltage at PCC.

At steady-state conditions, the output of the inverter is given by equations (11) and (12)

$$V_{di} = R_1 i_d^{'} - \omega L_1 i_q^{'} + V_d - \omega^2 L_1 C_1 V_d \tag{11}$$

$$V_{qi} = R_1 i_q^{'} + \omega L_1 i_d^{'} + \omega R_1 C_1 V_d \tag{12}$$

At PCC, the grid power real and reactive is specified by equations (13) and (14)

$$P(t) = V_d i_d \tag{13}$$

$$Q(t) = -V_d i_d \tag{14}$$

Finally, the real and reactive power supplied at PCC is given by equations (15) and (16)

$$P_{grid} = \frac{V_{qi}V_d}{\omega L_1} \tag{15}$$

$$Q_{grid} = \frac{V_{di}V_d - V_d^2}{\omega L_1} + \frac{V_d^2}{(1/\omega C_1)} \tag{16}$$

3. Implementation of BAS Controller and *d-q* Controller

The main objective proposed BAS controller is to extract the maximum generation from the PV cell and to improve the performance with the help of tuning the Proportional-Integral (PI) regulator. The usefulness of the BAS technique is operating in two ways one is to locate the operating point and the second is to tune the PI controller of the *d-q* controller.

3.1. BAS as MOP Controller

The effectiveness of the BAS controller is to track the operating point of solar PVS. The BAS technique is tuned to control the MOP to obtain the optimal duty cycle and to harvest maximum power generation from solar PVS modules. In the BAS technique, the behaviour of the beetle is discussed from Stage 1 to Stage 6 with its equation (1) – (7) in Section 2. The beetle behaviour is measured as random walk length and step size movement from one position to another position. The solar PVS power and duty cycle represent the suitability value and position of the beetle respectively. The sensing length antennae d^j and step size δ^j are calculated initially from equations (2) or (3) and (4) respectively. These calibrated parameters are fed to the input of BAS techniques to trace the MOP. At this stage, the solar PVS module voltage is equated to the voltage reference acquired from the BAS techniques to attain a MOP.

3.2. BAS Tuned d-q Controller

The BAS method presented in this research is also used for tuning the PI in the *d-q* controller to extract considerable power from the solar PVS. The BAS tuned *d-q* controller consists of two loops named as voltage and current loop with two PI regulators in each loop respectively as shown in Fig. 5. Each loop prefers an optimal value of PI regulators decided by BAS techniques for proportional gain (K_p) and integral gain (K_i). In routine, the BAS controller found three sets of values and by using a priori test to obtain an optimal gain value as given in Table 2.

The current loop allows precise active power to the grid; however, the voltage loop involves the preordained voltage reference suitable to the local loads. The *abc* and *αβ* transformation in the *d-q* controller converts the grid current and grid voltage into *d-q* components. The developed error from the aggregation of DC-link voltage (V_{dc}) and DC-link voltage reference (V_{dcref}) flows over the PI controller in a voltage loop. The DC-link voltage can be controlled by comparing the actual grid current of the *d-axis* (i_d) and the current controller of the *d-axis* (i'_d) provided by the output of the PI controller. Simultaneously, the *q-axis* can be estimated with grid voltage (V_{bus}) and the bus voltage reference (V_{busref}) like the *d-axis*.

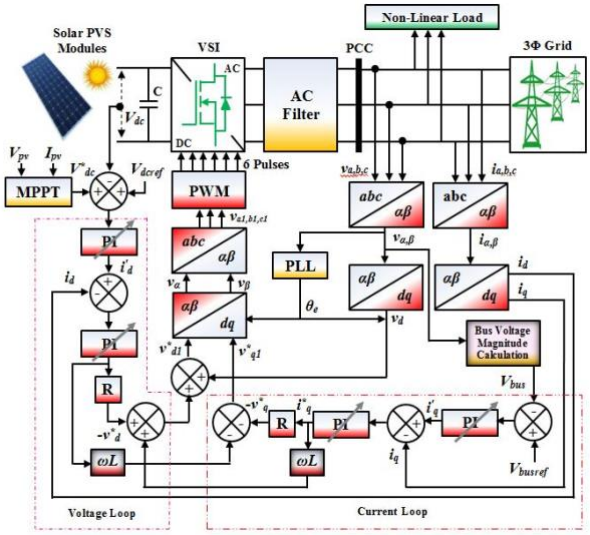

Fig. 5. Proposed e-BAS tuned *d-q* controller.

Table 2. Gain value of PI Regulator

Factor	K_p	K_i
Current Loop	0.963	291
Voltage Loop	0.978	225

The solar PVS obtains the reference voltage value in the current loop by means of $-v^*_d$ and $-v^*_q$ it can be raised up using the grid voltage as the new *d-q* voltage is specified by the equation (17) and (18)

$$V_{dnew} = Ri_d + L\frac{di_d}{dt} - \omega Li_q + v_\alpha \tag{17}$$

$$V_{qnew} = Ri_q + L\frac{di_q}{dt} - \omega Li_d + v_\beta \tag{18}$$

The variation of frequency in terms of both the phase value and theta value in solar PVS and grid are tracked by Phase Locked Loop (PLL) in Fig. 6. By using inverse park transformation the new *d-q* voltage is converted into *abc* voltage and current which is associated to the PWM modulator for the purposes of generating the gate pules to the VSI.

The main objective is to fine-tune the controller with BAS techniques in order to exclude the nonlinear state. Likewise, to maintain a continuous voltage across the capacitor (DC-link capacitor) for minimizing the error values based on equations (19) and (20).

For minimizing: $\left\{\left|V_{bus}-V_{bus}^{*}\right|\right\}$ (19)

This is subject to:

$$\left\langle\left|V_{dc}-V_{dc}^{*}\right|,\left\{\left(\frac{1}{\sqrt{3}}\sqrt{V_{d1}^{2}+V_{q1}^{2}}\right)\le\frac{1}{\sqrt{2}}\left(\frac{V_{dc}}{2}\right)\right\}\right\rangle \quad (20)$$

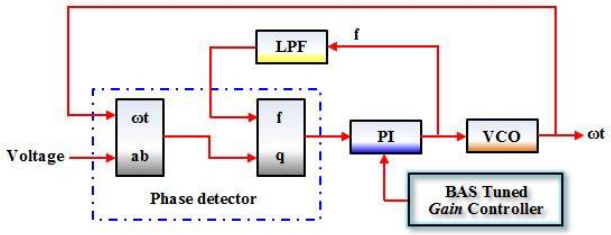

Fig. 6. Structure of PLL.

The modification of our research feature scaling factor is introduced in order to decrease the training data time of the steps as given in equation (21)

$$P_{ij}^{'}(t)=\frac{P_{ij}-\wedge\left(P_{ij}\right)}{\vee\left(P_{ij}\right)-\wedge\left(P_{ij}\right)} \quad (21)$$

where, $\vee\left(P_{ij}\right)$ and $\wedge\left(P_{ij}\right)$ – is minimum and maximum of steps value

These equations resolve the objective function of the proposed solar PVS for tuning the gain values of the controller by employing the e-BAS techniques with error minimization. To harvest the feasible amount of active and reactive power from solar PVS modules with the minimum fluctuations. Finally, the real and reactive power regulation is succeeded by constraints in equation (20) of operating the DC voltage control between the voltage reference (V^{*}_{dc}) and DC-link capacitor voltage (V_{dc}).

3.3. P-Q capability Curve of Solar PVS

The point (*P*, *Q*) originates the *P-Q* capability curve at the MOP condition. This curve enhances the sharing of reactive power at grid-tied solar PVS as shown in Fig. 7.

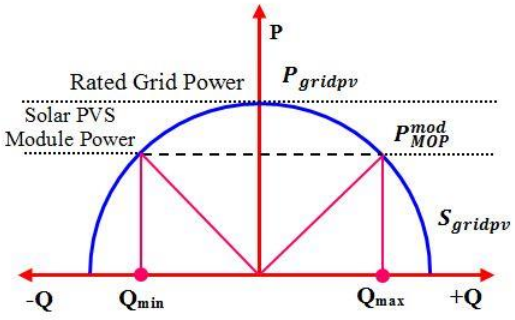

Fig. 7. *P-Q* capability curve with *Q* limits.

The capability curve depends on the power, voltage, and current rating of the solar PVS. Also, the active power depends on the rating and size of solar PVS modules. Based on the locality, the maximum power extracted from solar PVS modules depends on the solar irradiation (*G*) and the temperature (*T*) of the environment. The maximal harvesting power of Solar PVS at MOP is given by

$$P_{MOP}^{\mathrm{mod}}\left|G_{\max}T_{\min}=V_{MOP}I_{MOP}\right|G_{\max}T_{\min} \quad (22)$$

where, $G_{\max}T_{\min}$ – is the maximum G and minimum T at the locality of solar PVS, $V_{MOP}I_{MOP}$ – is the voltage and current at MOP of solar PVS and P_{MOP}^{mod} – is the module power at MOP of solar PVS.

The connected VSI of solar PVS is designed to habituate P_{MOP}^{mod}. This denotes that a solar PVS simplifies the transmission of extracted maximum workable power P_{MOP}^{mod} in the form of real power to the grid integration at unity PF. At the locality environment condition, the active and reactive power of capability of solar PVS is given by equations (23) and (24)

$$P_{gridpv}=\eta_{VSI}P_{MOP}^{\mathrm{mod}} \quad (23)$$

$$Q_{gridpv}=\sqrt{S_{gridpv}^{2}-P_{gridpv}^{2}} \quad (24)$$

where, η_{VSI} – is efficiency of VSI in solar PVS, $S_{gridpv}=P_{\max}$ – is power rating in MVA, and $\left(-Q_{gridpv},Q_{gridpv}\right)$ – is the range of reactive power limited in equation (24)

Also, the VSI output voltage in terms of the *d-q* reference frame with the solar PVS module is given by

$$V_{d,VSI}=\frac{V_{pv\,\mathrm{module}}}{2}m_i\cos\phi \quad (25)$$

$$V_{q,VSI}=-\frac{V_{pv\,\mathrm{module}}}{2}m_i\sin\phi \quad (26)$$

where, ϕ – is the phase angle of frequency in grid voltage and m_i – is the modulation index of grid-connected VSI

4. Implementation of BAS Controller and *d-q* Controller

4.1. Proposed Modeling of Solar PVS

The solar PVS has been preferred with 5 solar PVS modules with a series voltage of 37.1 V per module and the total series voltage (V_{pv}) of solar PVS is 185.5 V. The intended single-stage solar PVS contains solar PVS module cells, VSI, and AC filters with grid integration. The intended system achieves the imbalance voltage by enhancing the optimal gate pulse to VSI to attain a maximum power of solar PVS. The detailed modification is specified in this subsection to precise a standard analysis for the possibility to

perceive the intended e-BAS tuned *d-q* controller in solar PVS. The achieved performance analysis is tested in MATLAB/Simulink to harvest the maximum amount of solar power. This section gives the comparative study between the proposed system e-BAS tuned PI in *d-q* controller and ANOVA-tuned *d-q* controller. The parameter considered in this simulation for solar PVS configuration is specified in Table 3.

Table 3. Chosen parameters for solar PVS

Solar PVS	Factor	Ratings
AC Grid	Line voltage / frequency	11 kV / 50 Hz
VSI	Capacity / Voltage	120 kVA / 415 ± 1% V
Grid transformer	Voltage rating	415 V / 11 kV
PV system	Solar PVS identification	Refer the Table 1
Variable local load	Unbalanced load	60 kVA, lagging

4.2. Behaviour of Active and Reactive Power for e-BAS Tuned PI in d-q Controller

The grid performance of solar PVS is tested by choosing a temperature of 25°C with variable solar insolation. In this study, a constant current is assumed for an intended and conventional system. The variable solar irradiation pattern is considered with an increase and decrease in solar insolation from 700 W/m^2 to 1000 W/m^2 in the variation of 50 W/m^2, 100 W/m^2, and 150 W/m^2 are shown in Fig. 8(a). The predicted solar irradiance is measured by a solar power meter in our meteorological environments.

The dilemma of solar insolation variation is considered in the analysis by increase or decrease in variation as neither 50 W/m^2 nor 100 W/m^2 or 150 W/m^2 for every second. The solar PVS harvests the maximum amount of power from the solar PVS modules at MOP. The terminal voltage of the DC-link capacitor is controlled by VSI for the smooth function of grid integration. Fig. 8(b) illustrates the solar PVS module voltage for both the conventional and proposed system. The consequences of the intended and conventional systems are illustrated in Fig. 8(c) and Fig. 8(d) is a real and reactive power distributed by VSI to the grid integration.

Based on the illustration of active power the proposed e-BAS tuned PI *d-q* controller regulates the active power which is greater than the conventional system. Also, Table 4 specifies the comparison value of real power boosted to the grid and the Fig. 9 zoomed view gives clear evidence for regulated active power in proposed and conventional systems.

At normal operating conditions, the reactive power in the grid integration is regulated by maintaining the constant voltage at the PCC. But, when the high power penetration increases, it is a mandatory enhancement of real and reactive power regulation in grid integration. To eradicate this situation, a real power injection to the grid should be lesser than the rated capacity value of VSI. In such a way, the VSI is used for compensating the necessary reactive power injected into the grid. The constant voltage profile is maintained and the proposed e-BAS tuned *d-q* controller regulates the reactive power compensation which is better than the conventional system.

Table 4. Active power at variability conditions

Description	Irradiance (W/m^2)	Active Power in kW	
		Conventional System (ANOVA)	Proposed System (e-BAS)
Decreasing in step irradiance	100	106.8	108.0
	150	87.5	90.0
	50	81.8	84.0
Increasing in step irradiance	50	87.3	89.5
	150	105.7	107.8
	100	118.8	120.0

High priority is given to active power injection by the e-BAS tuned *d-q* controller of solar PVS and equation (21) controls the maximum possible reactive power compensation to the grid integration. The range of reactive power to the grid is limited by Q_{max} and Q_{min} which is decided by the obtainability of real power and the PF angle. The limitations consider for the reactive power compensation by the VSI are 10% to 100% of active power and 0 to 100% of reactive power with the rated value of solar PVS. Table 5 specifies the constraints of the VSI with the real and reactive power values. The tabularized value concludes that the e-BAS tuned *d-q* controller has better performances in voltage regulation than the conventional system.

4.3. Behaviour of Proposed Solar PVS in Grid Integration

The limited load environment of the proposed solar PVS is examined by variable solar irradiance. In an occurrence of zero power generation of solar PVS, the gird is segregated from solar PVS to exclude the grid blackouts. Moreover, the harvested solar PVS power is transmitted from VSI to the grid integration with the distortion in load observed by the proposed and conventional system was illustrates in Fig. 10. The grid voltage and grid current waveforms for the conventional and intended system in Fig. 10(a), Fig. 10(d), Fig. 10(c) and Fig. 10(f) respectively where the waveform is

twists out due to the non-linear loads at PCC for the conventional system.

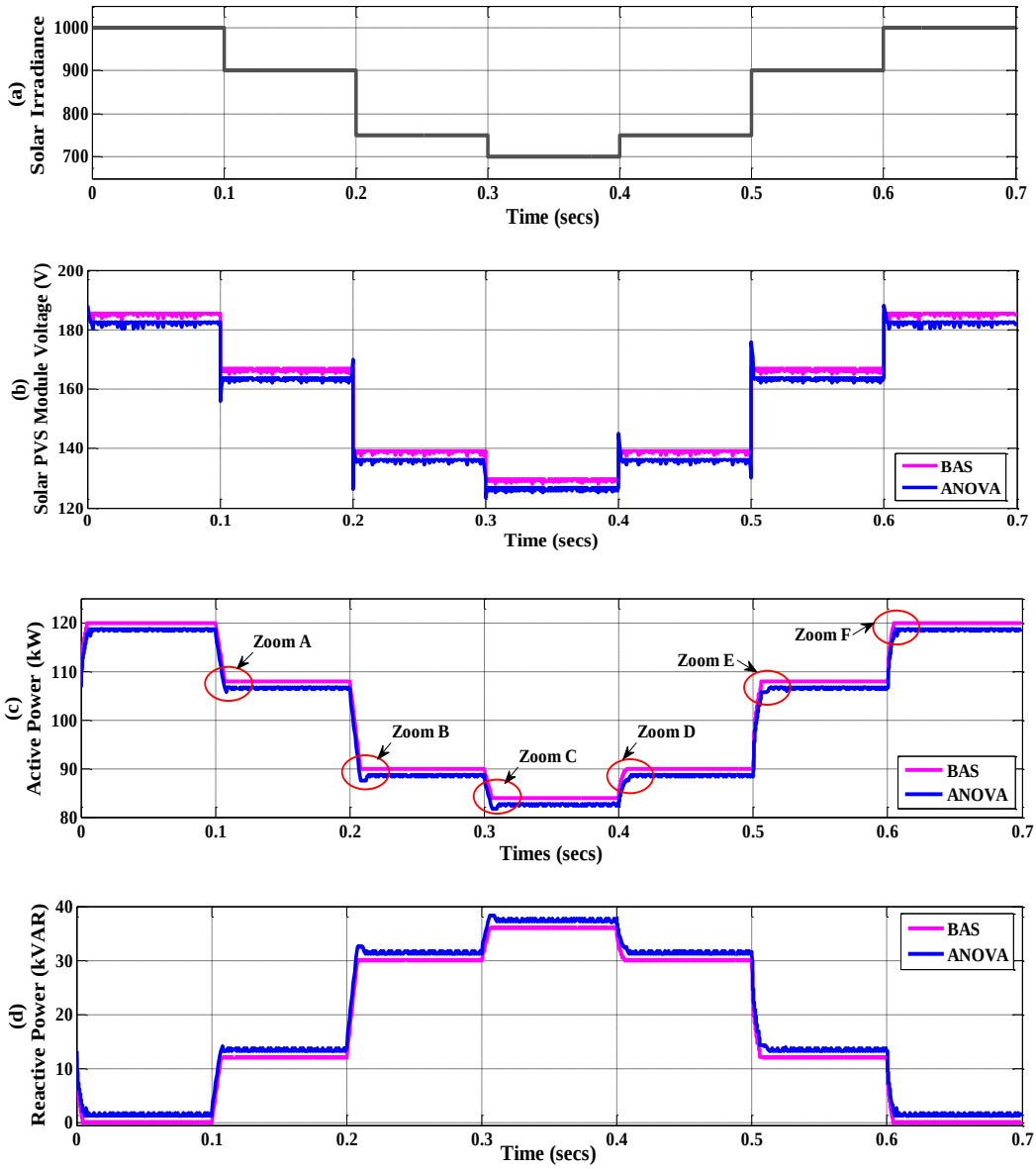

Fig. 8. (a) Patten of solar irradiance, (b) Solar PVS voltage, (c) Grid Active power of solar PVS in kW, (d) Grid Reactive power of solar PVS in kVAR.

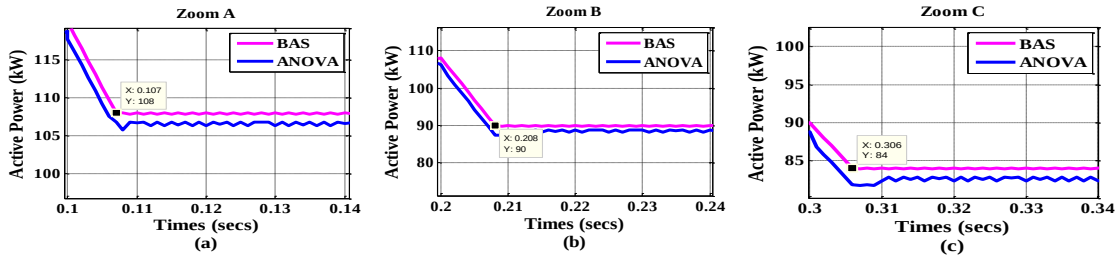

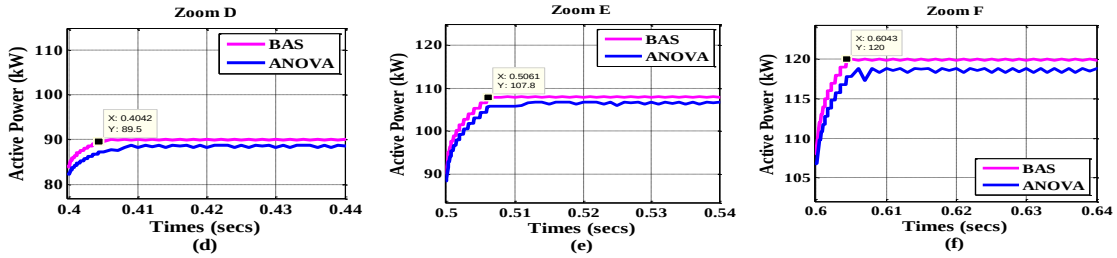

Fig. 9. Zoom view of active power at variability conditions.

Table 5. Comparison outcomes of P, Q, S and cos Φ

Limitations in%		P in kW		Q in kVAR		S in kVA		PF (cos Φ)	
P	**Q**	**ANOVA**	**e-BAS**	**ANOVA**	**e-BAS**	**ANOVA**	**e-BAS**	**ANOVA**	**e-BAS**
0	100	0	0	119.28	120	119.25	120	0	0
10	90	11.88	12.37	108.12	107.63	108.77	108.34	0.1092	0.1142
20	80	23.90	24.35	96.10	95.65	99.03	98.78	0.2413	0.2467
30	70	35.75	36.50	84.25	83.50	91.52	91.13	0.3906	0.4005
40	60	57.89	48.36	72.11	71.64	86.56	86.43	0.5532	0.5595
50	50	59.77	60.48	60.23	59.52	84.85	84.86	0.7044	0.7127
60	40	71.55	72.70	48.45	47.30	86.41	86.73	0.8280	0.8382
70	30	83.94	84.31	36.06.	35.69	91.36	91.55	0.9188	0.9209
80	20	95.71	96.54	24.29	23.46	98.74	99.35	0.9693	0.9717
90	10	107.83	108.42	12.17	11.58	108.51	109.04	0.9937	0.9943
100	0	119.76	120.49	0.24	0	119.76	120.49	0.9945	0.9967

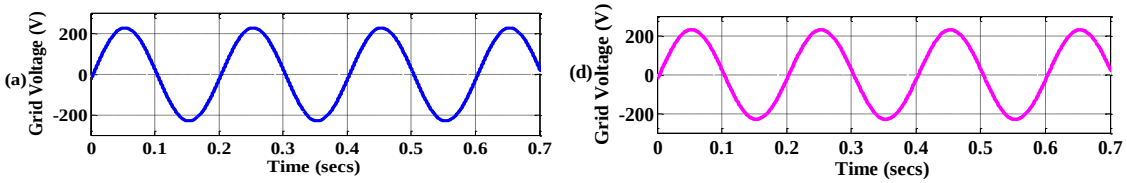

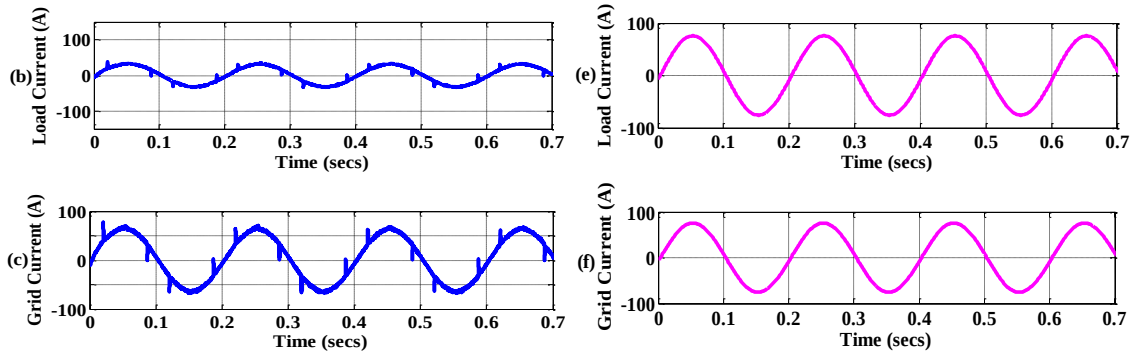

Fig. 10. Grid outcomes of solar PVS in per phase (a) Conventional Solar PVS Voltage (V), (b) Conventional Solar PVS Load current (A), (c) Conventional Solar PVS Grid Current (A), (d) Intended solar PVS Voltage (V), (e) Intended solar PVS Load current (A), (f) Intended solar PVS Current (A).

The achievable total harmonics distortions (THDs) of the conventional and intended system in terms of voltage THDs and current THDs are illustrated in Fig. 11 and Fig. 12. The conventional system voltage THDs is 0.12% and current THDs is 5.93% whereas the proposed system attained the voltage THDs of 0.09% and current THDs of 2.09%. It is found that the proposed e-BAS tuned *d-q* controller has low harmonic distortion than the conventional system and also the voltage and current THDs lie within the harmonic limits enforced by international standards.

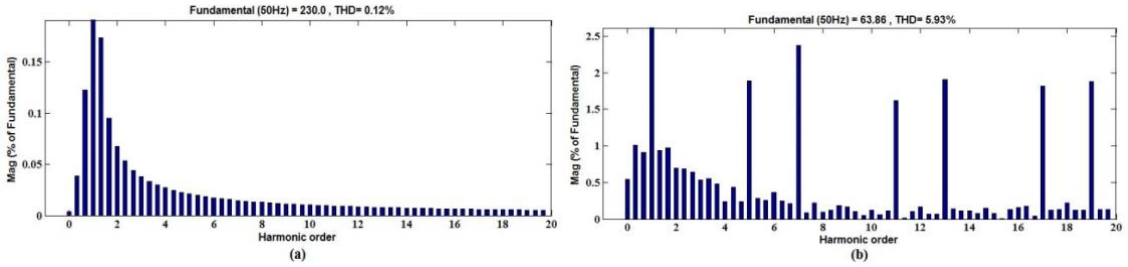

Fig. 11. THDs outcomes of conventional system (a) THDs of Solar PVS Voltage, (b) THDs of Solar PVS Currents.

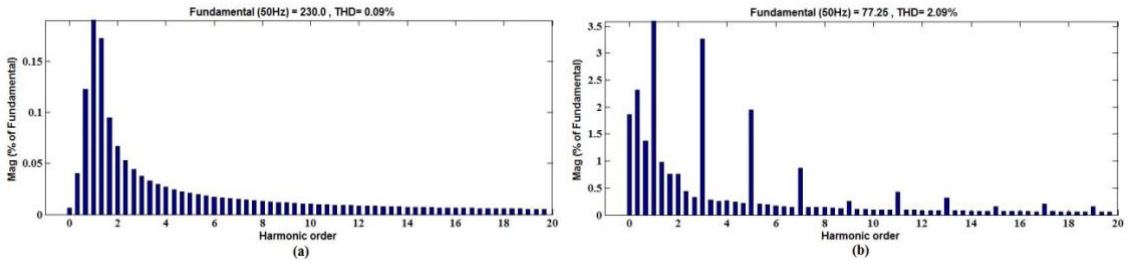

Fig. 12. THDs outcomes of intended system (a) THDs of solar PVS Voltage, (b) THDs of solar PVS Currents.

5. Conclusion

The grid integration of single-stage solar PVS has been evaluated for the reactive power compensation by using an e-BAS tuned *d-q* controller as a proposed system. An improved grid performance of active and reactive power is examined at the variability of environmental conditions. The proposed controller regulates grid voltage stability by limiting the reactive power from Q_{max} to Q_{min} based on the *P-Q* capability curves and also intended solar PVS carried out the holistic process at grid integration. The deterministic power harvesting is attained by sustaining the MOP at the variability conditions. The simulation illustrations and the tabulation are evidence of the superiority of the proposed e-BAS *d-q* controller over the conventional system. Therefore, voltage stability is achieved by controlling the real and reactive power by e-BAS tuned *d-q* controller as a proposed system. The grid analysis is proved in terms of voltage THDs as 0.09% and current THDs as 2.09% where the distortions lie within the limitation of international standards.

References

[1] M. Padmanaban, S. Chinnathambi, P. Parthasarathy, and N. Pachaivannan, "Extensive Study on Online, Offline and Hybrid MPPT Algorithms for Photovoltaic Systems," *Majlesi J. Electr. Eng.*, vol. 15, no. 3, pp. 1–16, Sep. 2021, doi: 10.52547/mjee.15.3.1.

[2] F. Javed, "Impact of Temperature & Illumination for Improvement in Photovoltaic System Efficiency," *Int. J. Smart Grid - IjSmartGrid*, vol. 6, no. 1, Art. no. 1, Mar. 2022.

[3] P. Chaudhary and M. Rizwan, "Voltage regulation mitigation techniques in distribution system with high

PV penetration: A review," *Renew. Sustain. Energy Rev.*, vol. 82, pp. 3279–3287, Feb. 2018, doi: 10.1016/j.rser.2017.10.017.

[4] M. Azab, "A finite control set model predictive control scheme for single-phase grid-connected inverters," *Renew. Sustain. Energy Rev.*, vol. 135, p. 110131, Jan. 2021, doi: 10.1016/j.rser.2020.110131.

[5] M. Colak and S. Balci, "Intelligent Techniques to Connect Renewable Energy Sources to the Grid: A review," in *2021 9th International Conference on Smart Grid (icSmartGrid)*, Jun. 2021, pp. 179–185. doi: 10.1109/icSmartGrid52357.2021.9551224.

[6] S. R. Das, P. K. Ray, A. K. Sahoo, K. K. Singh, G. Dhiman, and A. Singh, "Artificial intelligence based grid connected inverters for power quality improvement in smart grid applications," *Comput. Electr. Eng.*, vol. 93, p. 107208, Jul. 2021, doi: 10.1016/j.compeleceng.2021.107208.

[7] S. F. Zarei, H. Mokhtari, M. A. Ghasemi, S. Peyghami, P. Davari, and F. Blaabjerg, "DC-link loop bandwidth selection strategy for grid-connected inverters considering power quality requirements," *Int. J. Electr. Power Energy Syst.*, vol. 119, p. 105879, Jul. 2020, doi: 10.1016/j.ijepes.2020.105879.

[8] G. S. Rao, B. S. Goud, and Ch. R. Reddy, "Power Quality Improvement using ASO Technique," in *2021 9th International Conference on Smart Grid (icSmartGrid)*, Jun. 2021, pp. 238–242. doi: 10.1109/icSmartGrid52357.2021.9551226.

[9] N. Aouchiche, "Meta-heuristic optimization algorithms based direct current and DC link voltage controllers for three-phase grid connected photovoltaic inverter," *Sol. Energy*, vol. 207, pp. 683–692, Sep. 2020, doi: 10.1016/j.solener.2020.06.086.

[10] J. P. Roselyn, C. P. Chandran, C. Nithya, D. Devaraj, R. Venkatesan, V. Gopal, and S. Madhura, "Design and implementation of fuzzy logic based modified real-reactive power control of inverter for low voltage ride through enhancement in grid connected solar PV system," *Control Eng. Pract.*, vol. 101, p. 104494, Aug. 2020, doi: 10.1016/j.conengprac.2020.104494.

[11] C. Dang, X. Tong, and W. Song, "Sliding-mode control in dq-frame for a three-phase grid-connected inverter with LCL-filter," *J. Frankl. Inst.*, vol. 357, no. 15, pp. 10159–10174, Oct. 2020, doi: 10.1016/j.jfranklin.2019.12.022.

[12] A. Marrekchi, S. Keskes, S. Sallem, and M. B. A. Kammoun, "Comparative Analysis of Three Non-Linear Control Strategies for Grid-Connected PV System," *IETE J. Res.*, vol. 68, no. 5, pp. 3739–3749, Sep. 2022, doi: 10.1080/03772063.2020.1779617.

[13] G. M. Dousoky and M. Shoyama, "An AC MPPT with Active/Reactive Power Control Feature for Single-Stage Three-Phase Grid-Connected Photovoltaic VSIs," *Electr. Power Compon. Syst.*, vol. 45, no. 4, pp. 442–450, Feb. 2017, doi: 10.1080/15325008.2016.1266416.

[14] I. Owusu-Nyarko, K. H. Ahmed, F. Alsokhiry, and Y. Al-Turki, "Grid Interfacing of Multi-megawatt Photovoltaic System under Normal and Partial Shading Conditions," in *2021 9th International Conference on Smart Grid (icSmartGrid)*, Jun. 2021, pp. 118–123. doi: 10.1109/icSmartGrid52357.2021.9551238.

[15] S. Vlahinić, D. Franković, V. Komen, and A. Antonić, "Reactive Power Compensation with PV Inverters for System Loss Reduction," *Energies*, vol. 12, no. 21, Art. no. 21, Jan. 2019, doi: 10.3390/en12214062.

[16] N. Hamrouni, S. Younsi, and M. Jraidi, "A Flexible Active and Reactive Power Control Strategy of a LV Grid Connected PV System," *Energy Procedia*, vol. 162, pp. 325–338, Apr. 2019, doi: 10.1016/j.egypro.2019.04.034.

[17] M. Kashif, M. J. Hossain, F. Zhuo, and S. Gautam, "Design and implementation of a three-level active power filter for harmonic and reactive power compensation," *Electr. Power Syst. Res.*, vol. 165, pp. 144–156, Dec. 2018, doi: 10.1016/j.epsr.2018.09.011.

[18] H. Alenius, R. Luhtala, T. Messo, and T. Roinila, "Autonomous reactive power support for smart photovoltaic inverter based on real-time grid-impedance measurements of a weak grid," *Electr. Power Syst. Res.*, vol. 182, p. 106207, May 2020, doi: 10.1016/j.epsr.2020.106207.

[19] W. Yang, L. Chen, Z. Deng, X. Xu, and C. Zhou, "A multi-period scheduling strategy for ADN considering the reactive power adjustment ability of DES," *Int. J. Electr. Power Energy Syst.*, vol. 121, p. 106095, Oct. 2020, doi: 10.1016/j.ijepes.2020.106095.

[20] H. Özbay, S. Öncü, and M. Kesler, "SMC-DPC based active and reactive power control of grid-tied three phase inverter for PV systems," *Int. J. Hydrog. Energy*, vol. 42, no. 28, pp. 17713–17722, Jul. 2017, doi: 10.1016/j.ijhydene.2017.04.020.

[21] L. P. Sampaio, M. A. G. de Brito, G. de A. e Melo, and C. A. Canesin, "Grid-tie three-phase inverter with active power injection and reactive power compensation," *Renew. Energy*, vol. 85, pp. 854–864, Jan. 2016, doi: 10.1016/j.renene.2015.07.034.

[22] W. Qin, P. Wang, X. Han, and F. Meng, "Risk analysis of power systems for both real and reactive power," *J. Mod. Power Syst. Clean Energy*, vol. 1, no. 2, pp. 150–158, Sep. 2013, doi: 10.1007/s40565-013-0016-0.

[23] H. Benbouhenni, H. Gasmi, and N. Bizon, "Direct Reactive and Active Power Regulation of DFIG using an Intelligent Modified Sliding-Mode Control Approach," *Int. J. Smart Grid - IjSmartGrid*, vol. 6, no. 4, Art. no. 4, Dec. 2022.

[24] J. Huang, M. Liu, J. Zhang, W. Dong, and Z. Chen, "Analysis and field test on reactive capability of photovoltaic power plants based on clusters of inverters," *J. Mod. Power Syst. Clean Energy*, vol. 5, no. 2, pp. 283–289, Mar. 2017, doi: 10.1007/s40565-015-0154-7.

[25] V. F. Pires, A. Cordeiro, D. Foito, and J. F. Silva, "A DC-DC Converter with Capability to Support the Voltage Balance of DC Bipolar Microgrids," in *2022 11th International Conference on Renewable Energy Research and Application (ICRERA)*, Sep. 2022, pp. 50–55. doi: 10.1109/ICRERA55966.2022.9922819.

[26] S. Talkington, S. Grijalva, M. J. Reno, and J. A. Azzolini, "Solar PV Inverter Reactive Power Disaggregation and Control Setting Estimation," *IEEE*

Trans. Power Syst., vol. 37, no. 6, pp. 4773–4784, Nov. 2022, doi: 10.1109/TPWRS.2022.3144676.

[27] C. Wang, K. Zhang, J. Xiong, Y. Xue, and W. Liu, "A Coordinated Compensation Strategy for Module Mismatch of CHB-PV Systems Based on Improved LS-PWM and Reactive Power Injection," *IEEE Trans. Ind. Electron.*, vol. 66, no. 4, pp. 2825–2836, Apr. 2019, doi: 10.1109/TIE.2018.2842789.

[28] K. Çelik, M. Demirtas, and N. Öztürk, "Analytical Investigation of PV Panel Operated at Maximum Power Point on DC Microgrid," in *2022 11th International Conference on Renewable Energy Research and Application (ICRERA)*, Sep. 2022, pp. 324–329. doi: 10.1109/ICRERA55966.2022.9922864.

[29] S. Rahman, S. Saha, S. N. Islam, M. T. Arif, M. Mosadeghy, A. M. T. Oo, and M. E. Haque, "Analysis of Power Grid Voltage Stability with High Penetration of Solar PV Systems," in *2020 IEEE Industry Applications Society Annual Meeting*, Oct. 2020, pp. 1–8. doi: 10.1109/IAS44978.2020.9334716.

[30] Y. Fan, J. Shao, G. Sun, and X. Shao, "Improved Beetle Antennae Search Algorithm-Based Lévy Flight for Tuning of PID Controller in Force Control System," *Math. Probl. Eng.*, vol. 2020, p. e4287315, Mar. 2020, doi: 10.1155/2020/4287315.

[31] X. Xu, K. Deng, and B. Shen, "A beetle antennae search algorithm based on Lévy flights and adaptive strategy," *Syst. Sci. Control Eng.*, vol. 8, no. 1, pp. 35–47, Jan. 2020, doi: 10.1080/21642583.2019.1708829.

[32] S. Moonjerin, S. K. Ghosh, A. B. Bhadra, and A. K. Paul, "A Beetle Antenna Search based MPPT Algorithm for PV Systems Under Partially Shaded Condition," in *2019 IEEE International Conference on Power, Electrical, and Electronics and Industrial Applications (PEEIACON)*, Nov. 2019, pp. 19–22. doi: 10.1109/PEEIACON48840.2019.9071958.

[33] M. Padmanaban, S. Chinnathambi, P. Parthasarathy, and N. Pachaivannan, "Performance Evaluation of Active Power Correction Using BAS-PLC Controller for Solar Photovoltaic System," in *2022 International Conference on Smart Technologies and Systems for Next Generation Computing (ICSTSN)*, Mar. 2022, pp. 1–6. doi: 10.1109/ICSTSN53084.2022.9761301.

[34] M. Padmanaban, S. Chinnathambi, P. Parthasarathy, and N. Pachaivannan, "An e-ANOVA Tuned d-q Controller for Single Stage Grid Interface SPV system with Power Quality Improvement," *Int. J. Renew. Energy Res. IJRER*, vol. 11, no. 4, Art. no. 4, Dec. 2021.

[35] M. Padmanaban, S. Chinnathambi, P. Parthasarathy, and N. Pachaivannan, "Performance evaluation of improved ANOVA-tuned MPPT controlled DC–DC boost converter for SPV system," *Int. J. Electron.*, vol. 110, no. 7, pp. 1249–1266, Jul. 2023, doi: 10.1080/00207217.2022.2068668.